Progress In Electromagnetics Research, PIER 19, 109–127, 1998

RIGOROUS COUPLED WAVE THEORY OF ANISOTROPIC, AZIMUTHALLY-INHOMOGENEOUS CYLINDRICAL SYSTEMS

J. M. Jarem

Electrical and Computer Engineering Department
University of Alabama in Huntsville
Huntsville, AL 35899, USA

1. INTRODUCTION

A problem concerning circular cylindrical object scattering which has been studied is the problem of determining the scattering and radiation that occurs when a circular cylindrical dielectric system contains a region whose permittivity is inhomogeneous and periodic in the phi (φ) azimuthal direction [1–3]. Elsherbeni and Hamid [1] study EM, transverse magnetic (TM, electric field parallel to the cylinder axis) scattering from the inhomogeneous radial dielectric shell permittivity profile $\varepsilon(\rho,\varphi) = \varepsilon_a(\rho_0/\rho)^2(\eta - \delta\cos(2\varphi))$ where ε_a, ρ_0, η, and δ are constants defined in [1] and ρ and φ are cylindrical coordinates. Mathieu functions are used to solve for the EM fields in the inhomogeneous shell region. The choice of $\varepsilon(\rho,\varphi)$ used by [1–3] was necessary in order that the Region 2 solution could be expressed in terms of Mathieu functions. A limitation of the solution of [1–3] is the fact that their solution doesn't apply to an arbitrary $\varepsilon(\varphi,\varphi)$ profile, but only one to which a Mathieu function solution can be found.

In a recent paper [4] the present author generalized the work of [1–3] and presented an EM cylindrical solution algorithm to analyze radiation and scattering from isotropic dielectric cylindrical systems which have an arbitrary radial and azimuthal $\varepsilon(\varphi, \varphi)$ profile rather than the $\varepsilon(\rho, \varphi)$ profile used by [1–3]. The solution algorithm in this paper [4] was based on a recently developed EM planar diffraction grating algorithm called Rigorous Coupled Wave Theory [5–7]. The purpose of the present paper will be to further generalize the work [1–4] and extend the RCWT cylindrical algorithm of [4] to handle the analysis of anisotropic, inhomogeneous dielectric and permeable material cylinders. Other research on uniform anisotropic cylinder scattering may be found in [8, 9].

Specifically the algorithm of this paper will study the case when; (1) the electric field is polarized parallel to the material cylindrical axis (TM case), (2) the cylindrical scattering object has an arbitrary, isotropic, inhomogeneous, dielectric permittivity profile $\varepsilon(\rho, \varphi)$, and (3) the cylindrical scattering object has arbitrary, anisotropic inhomogeneous relative permeability tensor profiles $\mu_{xx}(x, y)$, $\mu_{xy}(x, y)$, $\mu_{yx}(x, y)$, $\mu_{yy}(x, y)$, (μ_{xz}, μ_{zx}, μ_{zy}, and μ_{yz} are taken to be zero). For the polarization of the present problem, the value of μ_{zz} is immaterial and therefore in this paper is not specified. Eqs (2, 3) of this paper and [9, 10] express the tensor elements in cylindrical components. The analysis of this paper also applies to the case when; (1) the magnetic field is polarized parallel to the cylindrical axis (TE case), (2) the cylindrical scattering object has an arbitrary, isotropic, inhomogeneous permeable profile $\mu(\rho, \varphi)$, and (3) the cylindrical scattering object has arbitrary, anisotropic inhomogeneous relative permittivity tensor profiles $\varepsilon_{xx}(x, y)$, $\varepsilon_{xy}(x, y)$, $\varepsilon_{yx}(x, y)$, and $\varepsilon_{yy}(x, y)$ (ε_{xz}, ε_{zx}, ε_{zy}, and ε_{yz}, are taken to be zero). This follows since the TE and TM cases just described are dual to one another.

The solution of this problem is of great interest in several areas of EM research. In the area of cylindrical aperture antenna theory, radial and azimuthal dielectric loading in front of a cylindrical aperture antenna can greatly alter, and therefore possibly enhance, the radiation characteristics of cylindrical aperture antennas [1–3]. Other EM applications include, (1) scattering from circular shaped, frequency-selective surfaces, (2) scattering from cylindrical surfaces covered with periodically spaced, inhomogeneous, anisotropic, radar absorbing material (RAM), (3) scattering from irregular shaped, inhomogeneous

mounting struts in an anechoic chamber, and (4) use as a cross check of other numerical algorithms (FD-TD or FE) which study scattering from inhomogeneous, anisotropic systems.

2. RIGOROUS COUPLED WAVE THEORY FORMULATION

This paper is concerned with the problem of determining the EM fields that arise when a plane wave and an off-center, interior line source excite EM fields in a circular cylindrical dielectric, anisotropic, permeability system as shown in Figs. 1–3 by using the RCWT method. The EM analysis will be carried out by; (1) solving Maxwell's equation in the interior and exterior regions of Figs. 1–3 in terms of cylindrical Bessel functions, (2) solving Maxwell's equation in the shell region by using a multi-layer state variable approach, and (3) matching EM boundary conditions at the interfaces. It is convenient to introduce normalized coordinates. We let $a = k_0\widetilde{a}$, $b = k_0\widetilde{b}$, $\rho = k_0\widetilde{\rho}$ etc. where unnormalized coordinates are in *meters* and $k_0 = 2\pi/\lambda$ is the free space wavenumber $(1/meters)$ and λ is the free space wavelength.

It is assumed that all fields and the medium are z-independent and that the relative dielectric permittivity in an inhomogeneous region of the material system is given by

$$\varepsilon(\rho,\varphi) = \sum_{i=-\infty}^{\infty} \breve{\varepsilon}_i(\rho) e^{ji\varphi}, \qquad 0 \le \varphi \le 2\pi \tag{1}$$

where $\breve{\varepsilon}_i(\rho)$ represent φ-exponential Fourier coefficients. The anisotropic permeability tensor is assumed to be given in rectangular and cylindrical coordinates by [9, 10]

$$\underline{\underline{\mu}} = \begin{bmatrix} \mu_{xx} & \mu_{xy} & 0 \\ \mu_{yx} & \mu_{yy} & 0 \\ 0 & 0 & \mu_{zz} \end{bmatrix}, \qquad \underline{\underline{\mu}} = \begin{bmatrix} \mu_{\rho\rho} & \mu_{\rho\varphi} & 0 \\ \mu_{\varphi\rho} & \mu_{\varphi\varphi} & 0 \\ 0 & 0 & \mu_{zz} \end{bmatrix} \tag{2}$$

where

$$\begin{aligned} \mu_{\rho\rho} &= \mu_{xx}\cos^2(\varphi) + (\mu_{xy} + \mu_{yx})\sin(\varphi)\cos(\varphi) + \mu_{yy}\sin^2(\varphi) \\ \mu_{\rho\varphi} &= \mu_{xy}\cos^2(\varphi) + (-\mu_{xx} + \mu_{yy})\sin(\varphi)\cos(\varphi) - \mu_{yx}\sin^2(\varphi) \\ \mu_{\varphi\rho} &= \mu_{yx}\cos^2(\varphi) + (-\mu_{xx} + \mu_{yy})\sin(\varphi)\cos(\varphi) - \mu_{xy}\sin^2(\varphi) \\ \mu_{\varphi\varphi} &= \mu_{yy}\cos^2(\varphi) + (-\mu_{xy} - \mu_{yx})\sin(\varphi)\cos(\varphi) + \mu_{xx}\sin^2(\varphi) \end{aligned} \tag{3}$$

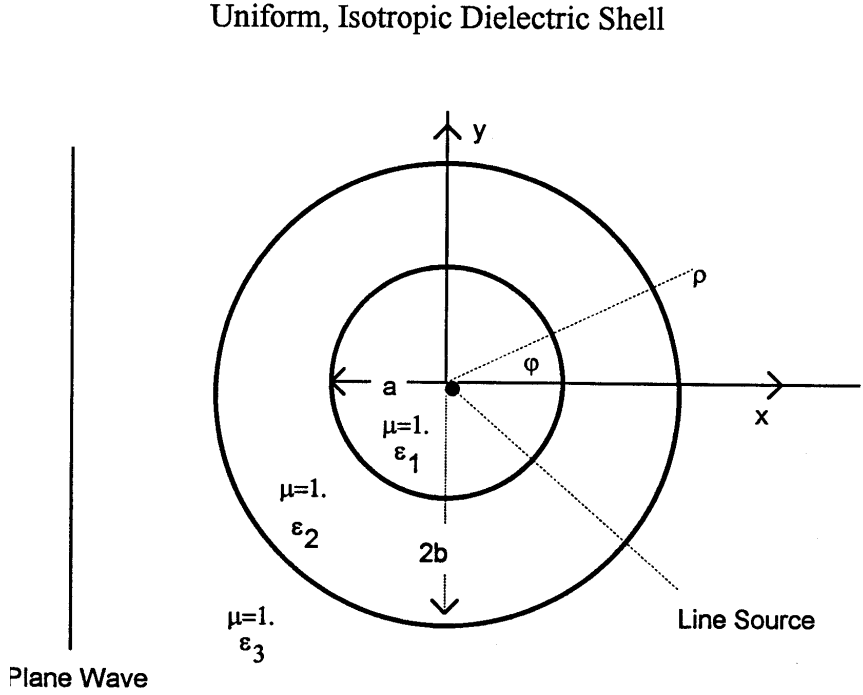

Figure 1. The geometry of uniform cylindrical shell system when a plane wave is incident on the cylindrical system and when an electric line source excites EM fields in the system is shown. The polarization of the electric field of the plane wave is parallel to the cylinder axis.

The cylindrical permeability tensor components are assumed to be expanded in the exponential Fourier series

$$\mu_{rs}(\rho,\varphi) = \sum_{i=-\infty}^{\infty} \breve{\mu}_{rs}(\rho) e^{ji\varphi} \qquad 0 \le \varphi \le 2\pi, \qquad (r,s) = (\rho,\varphi) \quad (4)$$

where $\breve{\mu}_{rs}(\rho)$ represents φ-exponential Fourier coefficients.

The EM fields interior and exterior (Regions 1 and 3 of Figs. 1 and 2) when a line source (Region 1) and a plane wave (Region 3) excite EM radiation in a cylindrical system are well known to be an infinite expansion of the Fourier-Bessel functions $H_n^{(2)} e^{jn\varphi}$, $J_n e^{jn\varphi}$, $Y_n e^{jn\varphi}$. Reference [4] gives a complete listing of the Fourier-Bessel expansions used subsequently in this paper.

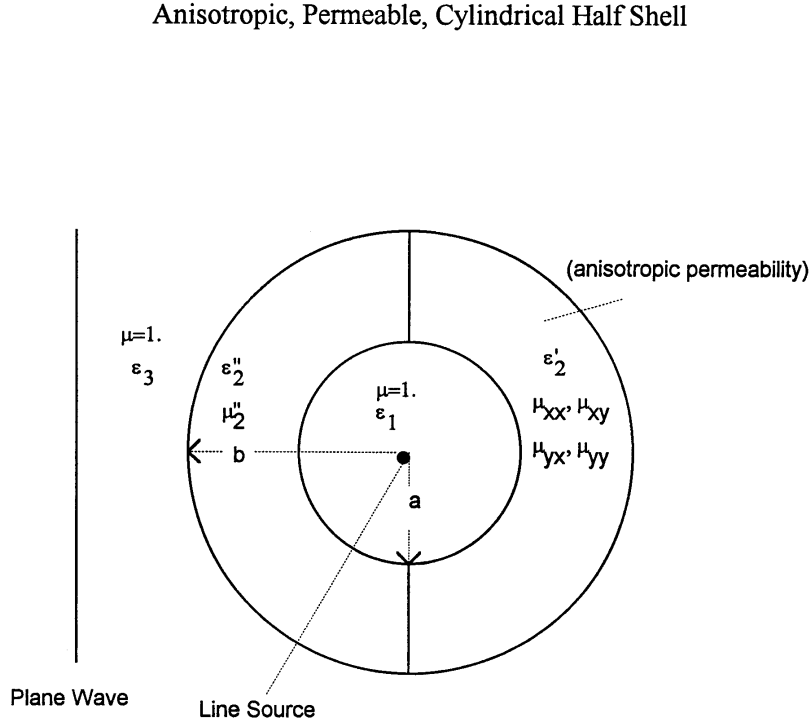

Figure 2. The geometry of an anisotropic, permeable, cylindrical half shell is shown along with a plane wave (electric field polarized parallel to the cylinder axis) and electric line source excitation.

In Region 2, the middle cylindrical dielectric region, we divide the dielectric region into L thin shell layers of thickness d_ℓ, $b-a = \sum_{\ell=1}^{L} d_\ell$ ($\ell = 1$ is adjacent to $\rho = b$ and $\ell = L$ is adjacent to $\rho = a$) and solve Maxwell's equations in cylindrical coordinates by a state variable approach in each thin layer. The layers are assumed to be thin enough in order that the ρ dependence of $\varepsilon(\rho,\varphi)$, $\mu_{\rho\rho}(\rho,\varphi)$, $\mu_{\rho\varphi}(\rho,\varphi)$, $\mu_{\varphi\rho}(\rho,\varphi)$ and $\mu_{\varphi\varphi}(\rho,\varphi)$ and the ρ scale factors may be treated as a constant in each layer. Making the substitutions $S_z = E_z$, $U_\rho = \eta_0 H_\rho$, and $U_\varphi = \eta_0 \rho H_\varphi$ where E_z, H_ρ, and H_φ represent the electric and magnetic fields in the thin shell region and $\eta_0 = 377\Omega$ is the intrinsic impedance of free space, we find that Maxwell's equations in a cylindrical shell of radius ρ are given by

$$\frac{\partial S_z}{\partial \varphi} = -j\rho\mu_{\rho\rho}U_\rho - j\mu_{\rho\varphi}U_\varphi \tag{5}$$

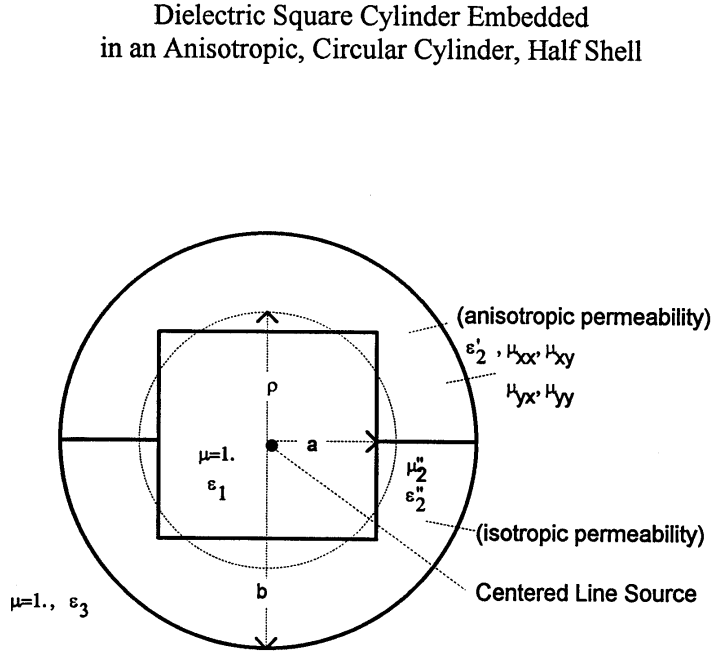

Figure 3. The geometry of an isotropic, dielectric, square cylinder embedded in an anisotropic, permeable, cylindrical half shell is shown along with an electric line source excitation.

$$\frac{\partial S_z}{\partial \rho} = j\mu_{\varphi\rho}U_\rho + j(\mu_{\varphi\varphi}/\rho)U_\varphi \tag{6}$$

$$\frac{\partial U_\varphi}{\partial \rho} - \frac{\partial U_\rho}{\partial \varphi} = j\rho\varepsilon S_z \tag{7}$$

To solve Eqs (5–7), we expand $S_z(\rho,\varphi)$, $U_\rho(\rho,\varphi)$, $U_\varphi(\rho,\varphi)$, $\varepsilon(\rho,\varphi)$, and $\mu_{rs}(\rho,\varphi)$, $(r,s) = (\rho,\varphi)$ in the Floquet harmonies:

$$S_z(\rho,\varphi) = \sum_{i=-\infty}^{\infty} s_{z_i}(\rho)e^{ji\varphi}, \qquad U_\rho(\rho,\varphi) = \sum_{i=-\infty}^{\infty} u_{\rho_i}(\rho)e^{ji\varphi},$$

$$U_\varphi(\rho,\varphi) = \sum_{i=-\infty}^{\infty} u_{\varphi_i}(\rho)e^{ji\varphi}, \quad \varepsilon(\rho,\varphi)E_z = \sum_{i=-\infty}^{\infty}\left[\sum_{i'=-\infty}^{\infty} \breve{\varepsilon}_{i-i'}s_{zi'}\right]e^{ji\varphi},$$

$$\mu_{rs}(\rho,\varphi)F(\rho,\varphi) = \sum_{i=-\infty}^{\infty}\left[\sum_{i'=-\infty}^{\infty} \breve{\mu}_{rs_{i-i'}}f_{i'}\right]e^{ji\varphi}, \ (r,s) = (\rho,\varphi) \tag{8}$$

where $F(\rho,\varphi)$ represents either $U_\rho(\rho,\varphi)$ or $U_\varphi(\rho,\varphi)$ in Eq (8) and f_i represents either u_{φ_i} or u_{ρ_i}. If these expansions are substituted in Eqs (5–7), and after letting $\underline{s_z}(\rho) = [s_{zi}(\rho)]$, $\underline{u_\rho}(\rho) = [u_{\rho i}(\rho)]$, and $\underline{u_\varphi}(\rho) = [u_{\varphi i}(\rho)]$ be column matrices and $\underline{\underline{\varepsilon}}(\rho) = [\breve{\varepsilon}_{i-i'}(\rho)]$, $\underline{\underline{\mu_{rs}}}(\rho) = [\breve{\mu}_{rs_{i-i'}}(\rho)]$, $(r,s) = (\rho,\varphi)$, $\underline{\underline{K}} = [K\delta_{i,i'}]$, $K = 2\pi \;/\; \Lambda_\varphi$ (Λ_φ is the circular grating period and $\delta_{i,i'}$ is the Kronecker delta) be square matrices we find after manipulation

$$\frac{\partial \underline{V}}{\partial \rho} = \underline{\underline{A}}\,\underline{V}, \qquad \underline{V} = \begin{bmatrix} \underline{s_z} \\ \underline{\mu_\varphi} \end{bmatrix}, \qquad \underline{\underline{A}} = \begin{bmatrix} \underline{\underline{A_{11}}} & \underline{\underline{A_{12}}} \\ \underline{\underline{A_{21}}} & \underline{\underline{A_{22}}} \end{bmatrix} \tag{9}$$

where

$$\underline{\underline{A_{11}}} = \frac{-j}{\rho}\underline{\underline{\mu_{\varphi\rho}}}\,\underline{\underline{\mu_{\rho\rho}}}^{-1}\underline{\underline{K}}, \qquad \underline{\underline{A_{12}}} = \frac{j}{\rho}(-\underline{\underline{\mu_{\varphi\rho}}}\,\underline{\underline{\mu_{\rho\rho}}}^{-1}\underline{\underline{\mu_{\rho\varphi}}} + \underline{\underline{\mu_{\varphi\varphi}}}),$$

$$\underline{\underline{A_{21}}} = j(-\frac{1}{\rho}\underline{\underline{K}}\,\underline{\underline{\mu_{\rho\rho}}}^{-1}\underline{\underline{K}} + \rho\underline{\underline{\varepsilon}}), \qquad \underline{\underline{A_{22}}} = \frac{-j}{\rho}\underline{\underline{K}}\,\underline{\underline{\mu_{\rho\rho}}}^{-1}\underline{\underline{\mu_{\rho\varphi}}}.$$

In these equations $\underline{u_\rho}$ was eliminated by finding the matrix inverse of $\underline{\underline{\mu_{\rho\rho}}}$, namely $\underline{\underline{\mu_{\rho\rho}}}^{-1}$, and then carrying out appropriate matrix multiplications. If Eq (9) is truncated at order M_T ($i = -M_T, \ldots, -1, 0, 1, \ldots, M_T$), Eq (9) represents a $N_T = 2(2M_T + 1)$ state variable equation (with matrix $(\underline{\underline{A}})_{N_T \times N_T}$). The solution of this equation is given by $\underline{V_n(\rho)} = \underline{V_n} e^{-q_n \rho}$ where q_n and $\underline{V_n}$ are the n^{th} eigenvalue and eigenvector of the constant matrix $\underline{\underline{A}}$. The quantities $\underline{\underline{A}}$, $\underline{V_n}$, and q_n satisfy $\underline{\underline{A}}\,\underline{V_n} = q_n \underline{V_n}$. The general EM fields in the ℓ_{th} thin shell region are given

$$E_z = \sum_{i=-M_T}^{M_T} \sum_{n=1}^{N_T} c_n s_{zin} e^{q_n \rho}, \qquad \eta_0 \rho H_\varphi = \sum_{i=-M_T}^{M_T} \sum_{n=1}^{N_T} c_n u_{\varphi in} e^{q_n \rho}, \tag{10}$$

where $\underline{V_n}^t = [\underline{s_{zn}^t}, \underline{u_{\varphi n}^t}]$ with $\underline{s_{zn}} = [s_{zin}]$ and $\underline{u_{\varphi n}} = [u_{\varphi in}]$ and where t represents matrix transpose.

Although a large matrix equation exists from which the overall solution of the problem may be obtained, a more efficient solution method is to use a ladder approach [6] (that is successively relate unknown coefficients from one layer to the next) to express the c_{nL} coefficients of the L^{th} last layer in terms of the c_{n1} coefficients of the first layer, and

then match boundary conditions at the $\rho = a$ and $\rho = b$ interfaces to obtain the final unknowns of the system. From [4] we obtain the following overall matrix equation

$$\underline{C}_L = \underline{\underline{F}}_{L-1}(\underline{\underline{F}}_{L-2} \cdots (\underline{\underline{F}}_1 \underline{C}_1)) = \underline{\underline{M}}\, \underline{C}_1 \tag{11}$$

$$\begin{aligned} c_0^I J_i(X_{1s}) = & \sum_{n=1}^{N_T} c_{nL} e^{-q_{nL} d_L} \left[-\frac{\pi J_i(X_{1a})}{2} \right] \\ & \left\{ ja\sqrt{\varepsilon_1} \frac{J_i'(X_{1a})}{J_i(X_{1a})} s_{zinL} + \mu_{\varphi inL} \right\} \end{aligned} \tag{12}$$

$$E_i^I = \sum_{n=1}^{N_T} c_{n1} \left[\frac{\pi H_i^{(2)}(X_{3b})}{2} \right] \left\{ jb\sqrt{\varepsilon_3} \frac{H_i^{(2)'}(X_{3b})}{H_i^{(2)}(X_{3b})} s_{zin1} + \mu_{\varphi in1} \right\}, \tag{13}$$

where $i = -M_T, \ldots, 0, \ldots, M_T$, $J'(X) = dJ(X)/dX$, etc., $X_{1s} = \sqrt{\varepsilon_1}\rho_s$, $X_{1a} = \sqrt{\varepsilon_1}a$, $X_{3b} = \sqrt{\varepsilon_3}b$, $E_i^I = E_0^I j^{-i}$, E_0^I is the incident plane wave amplitude, s_{zin1}, $u_{\varphi in1}$, s_{zinL}, and $u_{\varphi inL}$ are eigenvector components in the thin layers $\ell = 1$ and $\ell = L$ respectively, and $C_0^I = -\omega\mu_0 I/4$, where I is the line source excitation. (In [4] C_0^I was listed as $C_0^I = \omega\mu_0 I/4$. It should have been given as specified here.) Eq (12) represent a set of $2M_T + 1$ equations, Eq (13) represents a set of $2M_T + 1$ equations, and the matrix equation Eq (11) represents a set of $N_T = 2(2M_T + 1)$ equations. Thus Eqs (11–13) represent a set of $2N_T = 4(2M_T + 1)$ equations to calculate the $2N_T$ set of unknowns represented $\underline{C}_1$ and $\underline{C}_L$. Once these quantities are known all other unknown coefficients in the system may be found.

An important quantity to calculate is the normalized power of each order. We consider the important cases when the power is either radiated from the line source in Region 1 ($c_0^I \neq 0, E_0^I = 0$) or the power is scattered by a plane wave from Region 3 ($c_0^I = 0, E_0^I \neq 0$). In the case when $c_0^I \neq 0, E_0^I = 0$, the normalized power in each order is given [4] by $P_{Ni} = P_i^{RAD}/P^{INC}$ where P^{INC} is the incident power of the line source and P_i^{RAD} is the radiation at a radial distance ρ. For the plane wave scattering case ($c_0^I = 0, E_0^I \neq 0$), it is useful to calculate the normalized scattered at $\rho = \infty$ [4]

$$P_{Ni}^{Scat}(\infty) = (P_i^{Scat}(\infty)/\lambda)/S_{INC} \tag{14}$$

In Eq (14), S_{INC} is the power per unit area $(watts/meter^2)$ of the incident plane wave, and P_i^{scat} is the scattered power per unit length $(watts/m)$ of the i^{th} order.

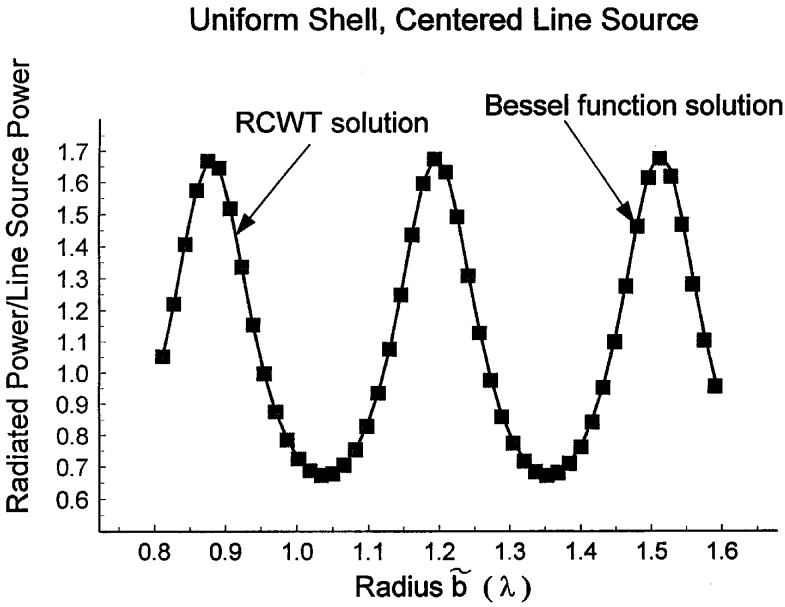

Figure 4. The normalized radiated power which results when a centered line source excites a uniform dielectric shell (see Fig. 1, $\varepsilon_1 = 1.5$, $\varepsilon_2 = 2.5$, $\varepsilon_3 = 1.$, $\mu = 1.$) is shown when determined by RCWT and when determined by a Bessel function matching solution.

3. NUMERICAL RESULTS

In this section we will study line source radiation and plane wave scattering using the RCWT method for three different material system examples.

The first example consists of studying line source radiation and plane wave scattering from a uniform dielectric shell. In this example all of space was taken to have a permeability $\mu = 1.$ and the permitivity in Regions 1, 2, 3 was taken to be respectively $\varepsilon_1 = 1.5$, $\varepsilon_2 = 2.5$, and $\varepsilon_3 = 1.$. The inner radius was taken to be $a = k_0\widetilde{a} = 5.$ ($\widetilde{a} = .795\lambda$) and the outer shell radius was taken to range from $b = a = 5.$ to $b = 10$. Using a centered line source excitation only (see Fig. 1), Fig. 4 shows a comparison of the normalized radiated power, (all normalized power in this section are assumed normalized either to the incident dipole or incident plane wave amplitude) as determined by the RCWT method (using $L = 10$ layers, $M_t = 1$) and

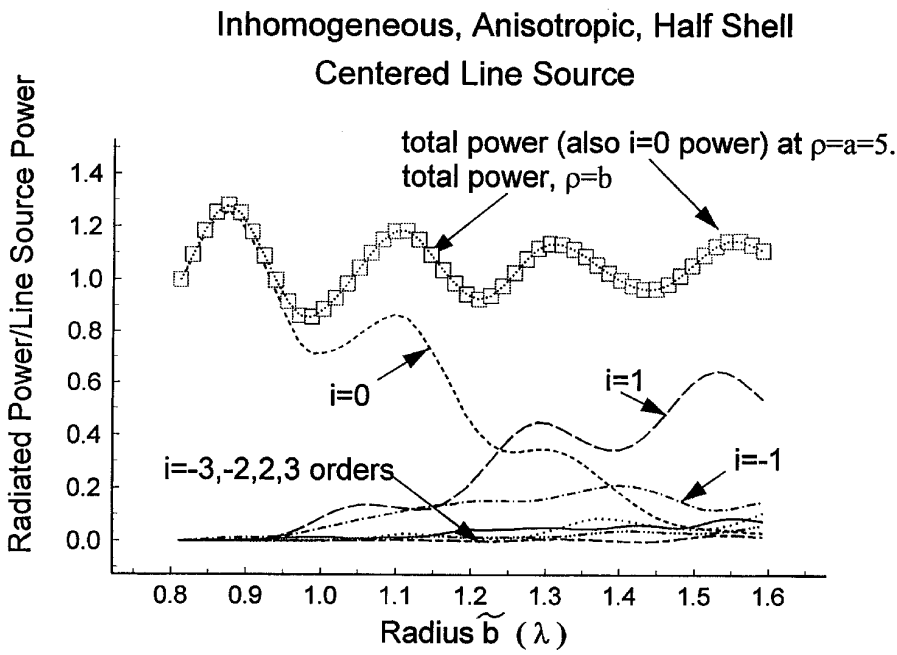

Figure 5. The total radiated power that results when a centered line source radiates through an anisotropic, permeable half shell (see Fig. 2, $\varepsilon_1 = 1.5$, $\varepsilon_3 = 1.$, $\varepsilon_2'' = 1.75$, $\mu_2'' = 1.5$, $\varepsilon_2' = 3.25$, $\mu_{xx} = 1.5$, $\mu_{xy} = .3$, $\mu_{yx} = .3$, $\mu_{yy} = 1.7$, $M_t = 10$, $L = 10$ layers) when the inner radius is $a = k_0\widetilde{a} = 5$ and when the outer radius is varied from $b = a = 5.$ to $b = 10.$ is shown.

as determined by a Bessel function matching solution method (based on matching Bessel function solutions in Regions 1, 2, 3) when the outer radius was varied from $b = a = 5.$ to $b = 10.$. As can be seen from Fig. 4, excellent agreement exists between the Bessel function matching algorithm and the RCWT method.

Fig. 5 shows the total radiated power that results when a centered line source radiates through an anisotropic, permeable half shell (see Fig. 2, $\varepsilon_1 = 1.5$, $\varepsilon_3 = 1.$, $\varepsilon_2'' = 1.75$, $\mu_2' = 1.5$, $\varepsilon_2' = 3.25$, $\mu_{xx} = 1.5$, $\mu_{xy} = .3$, $\mu_{yx} = .3$, $\mu_{yy} = 1.7$, $M_t = 10$, $L = 10$ layers) when the inner radius is $a = k_0\widetilde{a} = 5$ and when the outer radius is varied from $b = a = 5$ to $b = 10$. As can be seen almost exact conservation of power at the inner and outer radius is observed. At

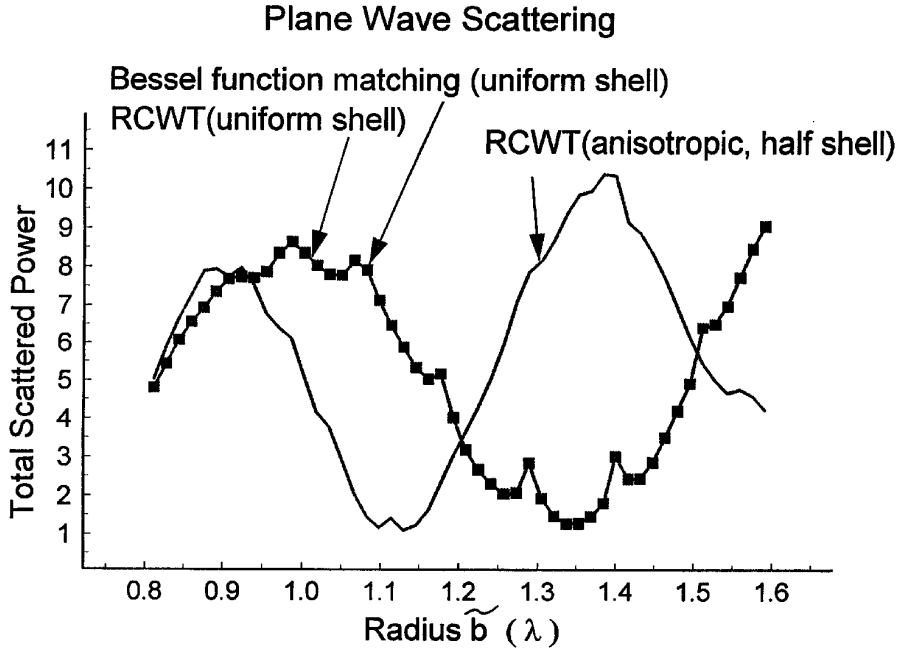

Figure 6. A comparison of the total plane wave power scattered by the same uniform dielectric shell example as considered in Fig. 4 (see Fig. 1, assume the centered line source not present) as determined by the Bessel function matching solution ($M_t = 15$) and as determined by the RCWT method (using $L = 15$ layers, $M_t = 15$) is shown. Plane wave scattering from an anisotropic cylinder is also shown.

$\rho = a$ (inner radius) no power was calculated to be diffracted into higher orders. This is why the total power at $\rho = a$ also equals the $i = 0$ power at $\rho = a$. Also shown in Fig. 5 are the $i = -1$, $i = 0$, $i = 1$ orders radiated at $\rho = b$ (outer radius) and the higher orders $i = -3, -2, 2, 3$. As $\widetilde{b}$ is increased from $\widetilde{b} = .8\lambda$ to $\widetilde{b} = 1.6\lambda$ in Fig. 5, one clearly observes that as the outer radius is increased, power is depleted out of the $i = 0$ order and is diffracted into higher orders. One also observes that unequal order power is radiated into the $i = -1$ and the $i = 1$ orders. This is to be expected and is a result of the anisotopy of the permeable half shell.

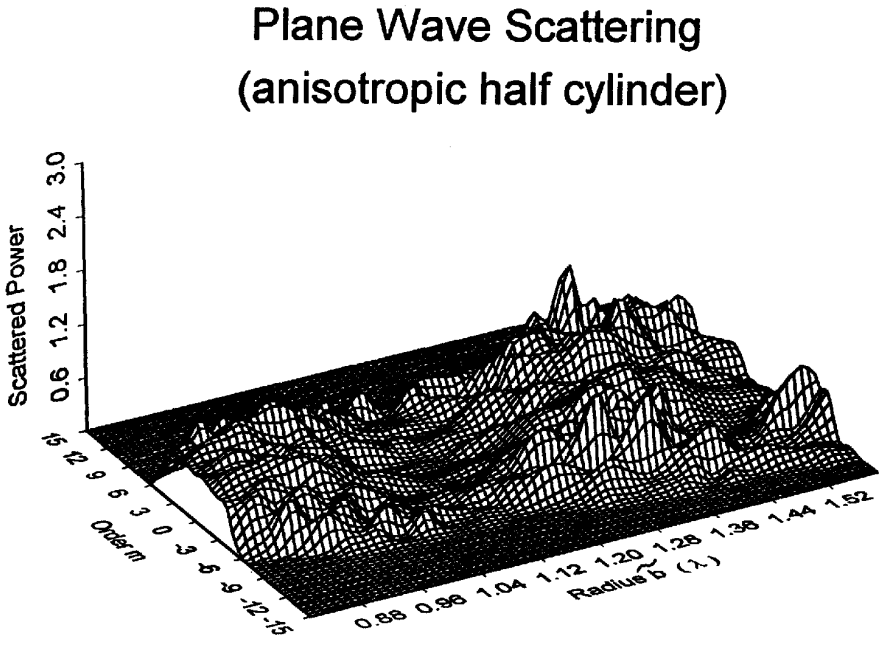

Figure 7. A three dimensional plot of the plane wave scattered order power verses order i when i is varied from $i = -15$ to $i = 15$ and verses the outer radius $\widetilde{b}$ when $\widetilde{b}$ is varied from $\widetilde{b} = .8\lambda$ to $\widetilde{b} = 1.6\lambda$ is shown. Fig. 7 is part of the same numerical case as was studied in Fig. 6.

Figs. 6–8 display scattering results when a plane wave is incident on the cylindrical system. Fig. 6 (*solid line* and *square*) shows a comparison of the total plane wave power scattered by the same uniform dielectric shell example as considered in Fig. 4 (see Fig. 1, assume the centered line source not present) as determined by the Bessel function matching solution (*square,* $M_t = 15$) and as determined by the RCWT method (*solid line,* using $L = 15$ layers, $M_t = 15$). As can be seen from Fig. 6, excellent agreement was obtained between the two methods. As can be seen from Fig. 6, the RCWT method was able to accurately reproduce even the small resonance peaks that arise in the scattering solution. Fig. 6 (*solid line* labeled *RCWT (anisotropic, half shell)*) shows the total plane wave scattered power (as a function

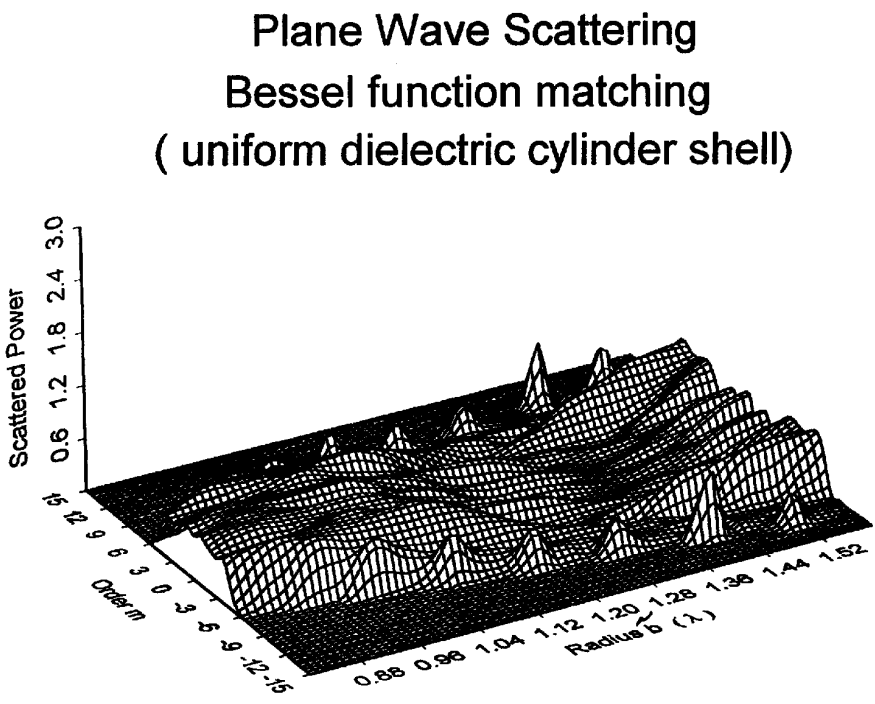

Figure 8. The scattered order power that occurs when a plane wave impinges on a uniform dielectric shell (see FIg. 1, $\varepsilon_1 = 1.5$, $\varepsilon_2 = 2.5$, $\varepsilon_3 = 1.$, $\mu = 1.$) rather than an anisotropic half shell is shown.

of the outer radius $\widetilde{b}$) that results when a plane wave is incident on an anisotropic, permeable cylindrical half shell (see Fig. 2, $\varepsilon_1 = 1.5$, $\varepsilon_3 = 1.$, $\varepsilon_2'' = 1.75$, $\mu_2'' = 1.5$, $\varepsilon_2' = 3.25$, $\mu_{xx} = 1.5$, $\mu_{xy} = .3$, $\mu_{yx} = .3$, $\mu_{yy} = 1.7$, $M_t = 15$, $L = 15$ layers). As can be seen from Fig. 6, the presence of the anisotropic, half shell causes a significantly different scattering profile than does the isotropic, uniform shell cylinder.

Fig. 7 shows a three dimensional plot of the plane wave scattered order power verses order i when i is varied from $i = -15$ to $i = 15$ and verses the outer radius $\widetilde{b}$ when $\widetilde{b}$ is varied from $\widetilde{b} = .8\lambda$ to $\widetilde{b} = 1.6\lambda$. Fig. 7 is part of the same numerical case as was studied in Fig. 6. As can be seen from Fig. 7, one clearly observes asymmetry of the order power as the size of the outer radius $\widetilde{b}$ is increased. The sum

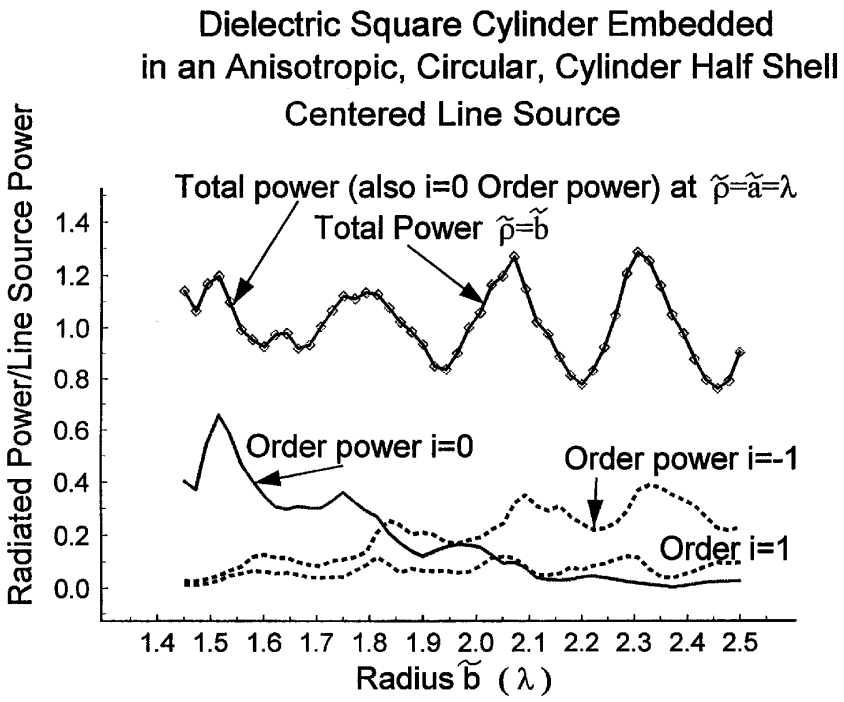

Figure 9. The total radiated power (normalized to the dipole power of the centered line source) when a line source radiates from an isotropic square cylinder which is embedded in an anisotropic permeable half shell (see Fig. 3, $\varepsilon_1 = 1.5$, $\varepsilon_3 = 1.$, $\varepsilon_2'' = 3.5$, $\mu_2'' = 1.$, $\varepsilon_2' = 3.25$, $\mu_{xx} = 1.5$, $\mu_{xy} = .3$, $\mu_{yx} = .3$, $\mu_{yy} = 1.7$, $M_t = 20$, $L = 25$ layers).

of the plane wave order power at any given $\widetilde{b}$ gives the total scattered power which is displayed in Fig. 6. We again note that this total plane wave scattered power obeys conservation of power as expected. Fig. 8 for comparison with Fig. 7, shows the scattered order power that occurs when a plane wave impinges on a uniform dielectric shell ($\varepsilon_1 = 1.5$, $\varepsilon_2 = 2.5$, $\varepsilon_3 = 1.$, $\mu = 1.$) rather than an anisotropic half shell. The uniform dielectric shell has dielectric permittivity values which are roughly the same size as the that of the anisotropic half shell. As can be seen from Fig. 8, the three dimensional shape of the Fig. 8 plot from the uniform shell is symmetric in the order parameter i and in general has quite a different shape than that of the anisotropic half shell in Fig. 7.

Fig. 9 shows the total radiated power (normalized to the dipole power of the centered line source) when a line source radiates from an isotropic square cylinder which is embedded in an anisotropic permeable half shell (see Fig. 3, $\varepsilon_1 = 1.5$, $\varepsilon_3 = 1.$, $\varepsilon_2'' = 3.5$, $\mu_2'' = 1.$, $\varepsilon_2' = 3.25$, $\mu_{xx} = 1.5$, $\mu_{xy} = .3$, $\mu_{yx} = .3$, $\mu_{yy} = 1.7$, $M_t = 20$, $L = 25$ layers). The radiated power was calculated at $\rho = a$ ($\widetilde{a} = 1.\lambda$) which is a circle enscribed in the square cylinder of Region 1 and was calculated at $\rho = b$ ($\widetilde{b} = 2.5\lambda$) which is the outer radius of the anisotropic half cylinder. The outer radius $\widetilde{b}$ was varied from $\widetilde{b} = \sqrt{2}\widetilde{a} = 1.414\lambda$ to $\widetilde{b} = 2.5\lambda$. As can be seen from Fig. 9, extremely good power conservation was observed at $\rho = a$ ($\widetilde{a} = 1\lambda$) and at $\widetilde{\rho} = \widetilde{b}$. Despite the square shape of the cylinder, no power was observed to be diffracted into higher orders at $\rho = a$ ($\widetilde{a} = 1\lambda$). Also show in Fig. 9 are the $i = -1$, $i = 0$, $= 1$ orders radiated at $\rho = b$ (outer radius). As in Fig. 7, one observes that power is depleted from the $i = 0$ order and radiated into higher orders. Fig. 9 shows the increase in the $i = -1$ and $i = 1$ orders, for example, that occurs when $\widetilde{b}$ is increased. One also observes in Fig. 9 that the order power is radiated asymmetrically into the $i = -1$ and $i = 1$ orders. As in Fig. 7 this is expected and is due to the anisotropy of the permeable half shell.

Fig. 10 shows a plot (*dotted line*) of the relative dielectric permittivity function $\varepsilon(\rho, \varphi)$ when $\widetilde{\rho} = 1.241\lambda$ for the square cylinder-anisotropic, half shell case displayed in Fig. 3. The circular dashed line of Fig. 3 represents the approximate placement of $\widetilde{\rho} = 1.241\lambda$ parameter used to make the Fig. 10 $\varepsilon(\rho, \varphi)$ plots. Also shown in Fig. 10 (*solid line*) is the Fourier series representation of the $\varepsilon(\rho, \varphi)$ profile when $\widetilde{\rho} = 1.241\lambda$ and $M_t = 20$. ($M_t = 20$ was used to make the RCWT analysis of Fig. 9.). As can be seen from Fig. 9, enough Fourier terms ($-40 = -2M_t \leq i \leq 2M_t = 40$) were used in order to correctly model the inhomogeneous region as defined by the square cylinder. (Note: The convolution matrix of Eq (8) requires $2M_t = 40$ terms.) Figs. 11–13 shows the relative permeability tensor profiles $\mu_{\rho\rho}(\rho, \varphi)$, $\mu_{\rho\varphi}(\rho, \varphi)$, $\mu_{\varphi\rho}(\rho, \varphi)$ $\mu_{\varphi\varphi}(\rho, \varphi)$ for the same case and parameters as shown in Fig. 10. The numerical example of Fig. 9 was chosen such that $\mu_{\rho\varphi}(\rho, \varphi) = \mu_{\varphi\rho}(\rho, \varphi)$.

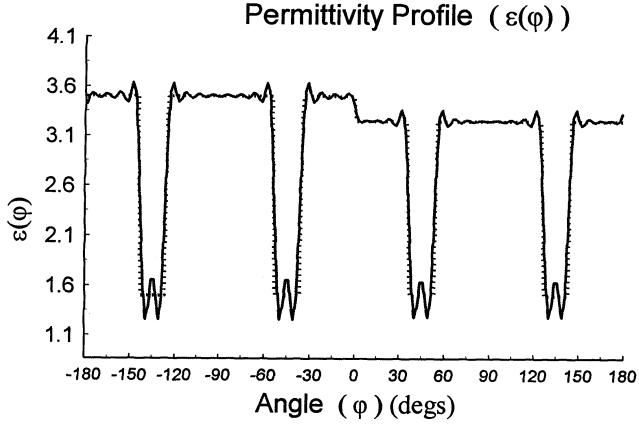

Figure 10. A plot (*dotted line*) of the relative dielectric permittivity function $\varepsilon(\rho, \varphi)$ when $\widetilde{\rho} = 1.241\lambda$ for the square cylinder-anisotropic, half shell case displayed in Fig. 3 is shown. The circular dashed line of Fig. 3 represents the approximate placement of $\widetilde{\rho} = 1.241\lambda$ parameter used to make the Fig. 10 $\varepsilon(\rho, \varphi)$ plots. Also shown in Fig. 10 (*solid line*) is the Fourier series representation of the $\varepsilon(\rho, \varphi)$ profile when $\widetilde{\rho} = 1.241\lambda$ and $M_t = 20$. ($M_t = 20$ was used to make the RCWT analysis of Fig. 9.).

4. SUMMARY

A state variable EM analysis technique called rigorous wave coupled theory (RCWT) has been applied to determine radiation and scattering that arises from circular cylindrical, anisotropic inhomogeneous material systems. The work represents a generalization of the work performed: (1) by Elsherbeni and Hamid [1, 2] and Elsherbeni and Tew [3] who studied an inhomogeneous sinusoidal circular cylindrical system whose EM field solutions were Mathieu functions, (2) by Wu [9, 10] who considered scattering from homogeneous anisotropic dielectric cylinders using a Bessel function approach, and (3) by Jarem [4] who used the RCWT method to determine radiation and scattering from isotropic, inhomogeneous dielectric systems. The RCWT state matrix equations and the associated boundary matrix equations (derived from a multi-layer ladder analysis) are presented and solved for the first time for the cases when a plane wave (TM polarization, electric field parallel to the cylinder axis) or electric line source is incident on a cylinder which possesses an inhomogeneous permitivitty profile

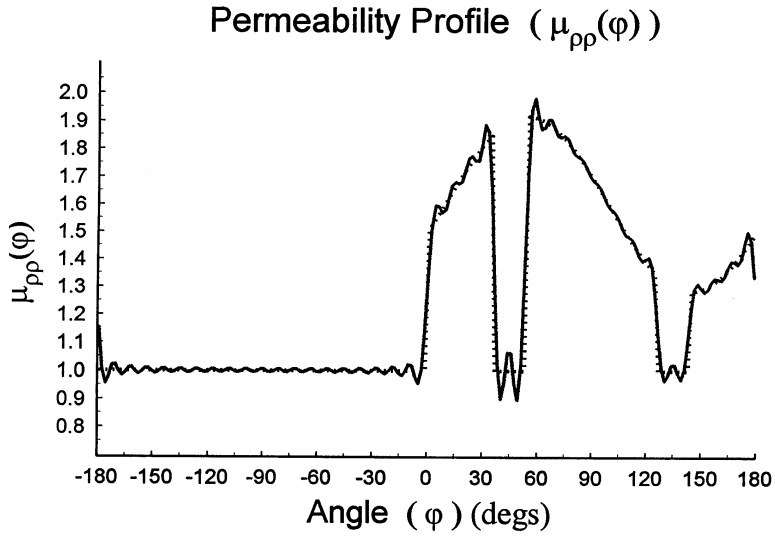

Figure 11. Plots of the relative permeability function $\mu_{\rho\rho}(\rho, \varphi)$ (exact (*dotted line*) and Fourier series representation (*solid line*)) for the same case as described in Fig. 10 are shown.

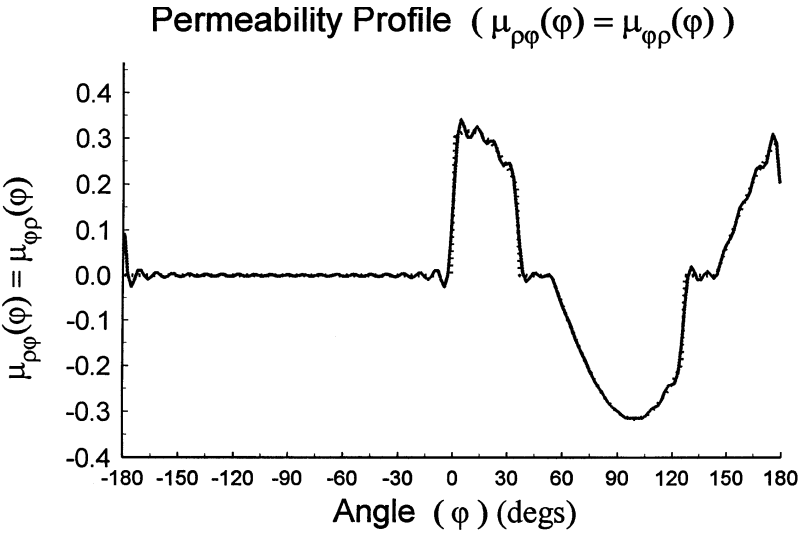

Figure 12. Plots of the relative permeability function $\mu_{\rho\varphi}(\rho, \varphi) = \mu_{\varphi\rho}(\rho, \varphi)$ (exact (*dotted line*) and Fourier series representation (*solid line*)) for the same case as described in Fig. 10 are shown.

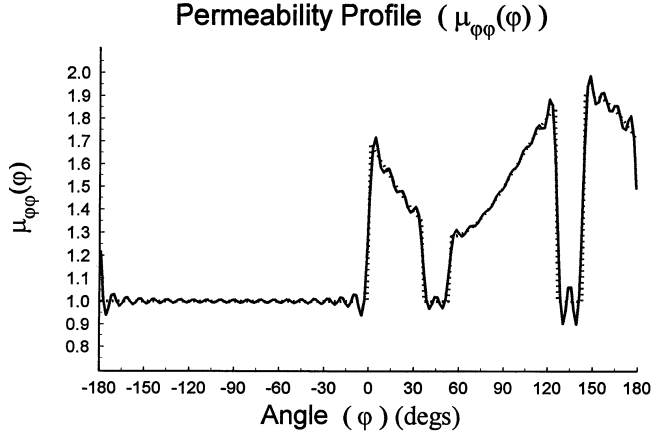

Figure 13. Plots of the relative permeability function $\mu_{\varphi\varphi}(\rho, \varphi)$ (exact (*dotted line*) and Fourier series representation (*solid line*)) for the same case as described in Fig. 10 are shown.

$\varepsilon(\rho, \varphi)$ and possesses inhomogeneous, anisotropic permeability profiles $\mu_{\rho\rho}(\rho, \varphi)$, $\mu_{\rho\varphi}(\rho, \varphi)$, $\mu_{\varphi\rho}(\rho, \varphi)$, and $\mu_{\varphi\varphi}(\rho, \varphi)$. As mentioned in the Introduction the results of this paper also hold for the electromagnetic case which is dual to the one which has been studied.

In general the RCWT algorithm presented herein can be modified to study the cases when the inner region is a perfect conductor, when the permittivity and permeability is anisotropic or bi-anisotropic, and can be modified to study the cases when the incident polarization may be both TE, TM, and oblique. The RCWT algorithm can also be modified to study the scattering that occurs when a plane wave or line source is obliquely incident on a crossed periodic cylinder, namely a cylinder system which is periodic in both the phi (φ) and longitudinal z directions. This problem is analogous to planar crossed diffraction grating analysis. The present author also believes that a multi-layer RCWT version of the present algorithm as also mentioned in [4] will be ideal for massively parallel computations (and have good load balance) since one can perform the eigenanalysis of many cascaded cylindrical thin layers in parallel. The present authors has applied the RCWT method to study radiation and scattering from three dimensional inhomogeneous objects, specifically an inhomogeneous spherical system [11]. Future work by the author will concentrate on some of the just mentioned topics.

REFERENCES

1. Elsherbeni, A. Z., and M. Hamid, "Scattering by a cylindrical dielectric shell with inhomogeneous permittivity profile," *Int. J. Electronics,* Vol. 58, No. 6, 949–962, 1985.
2. Elsherbeni, A. Z., and M. Hamid, "Scattering by a cylindrical dielectric shell with radial and azimuthal permittivity profiles," *Proc. 1985 Symp. Of Microwave Technology in Industrial Development,* 77–80, Brazil July 22-25, 1985 (Invited).
3. Elsherbeni, A. Z., and M. Tew, "Electromagnetic scattering from a circular cylinder of homogeneous dielectric coated by a dielectric shell with a permittivity profile in the radial and azimuthal directions-even TM case," *IEEE Proceedings-1990 Southeastcon,* Session 11A1, 996–1000.
4. Jarem, J. M., "Rigorous coupled wave theory solution of phi-periodic circular cylindrical dielectric systems," *Journal of Electromagnetic Waves and Applications,* Vol. 11, 197–213, 1997.
5. Moharam, M. G., and T. K. Gaylord, "Rigorous coupled-wave analysis of planar grating diffraction," *J. Opt. Soc. Amer.,* Vol. 71, 811–818, 1981.
6. Moharam, M. G., and T. K. Gaylord, "Diffraction analysis of dielectric surface-relief gratings," *J. Opt. Soc. Amer.,* Vol. 72, 1385–1392, 1987.
7. Rokushima, K., J. Yamakita, S. Mori, and K. Tominaga, "Unified approach to wave diffraction by space-time periodic anisotropic media," *IEEE Trans. on Microwave Theory and Techniques,* Vol. 35, 937–945, 1987.
8. Glytsis, E. N., and T. K. Gaylord, "Rigorous three-dimensional coupled-wave diffraction analysis of single cascaded anisotropic gratings," *J. Opt. Soc. Amer. A,* Vol. 4, No. 11, 2061–2080, 1987.
9. Wu, X. B., "Scattering from an anisotropic cylindrical dielectric shell," *International Journal of Infrared and Millimeter Waves,* Vol. 15, No. 10, 1733–1743, 1994.
10. Wu, X. B., "An alternative solution of the scattering from an anisotropic cylindrical dielectric shell," *International Journal Of Infrared and Millimeter Waves,* Vol. 15, No. 10, 1745–1754, 1994.
11. Jarem, J. M., "Rigorous coupled-wave-theory analysis of dipole scattering from a three-dimensional, inhomogeneous, spherical dielectric and permeable system," *IEEE Microwave Theory and Techniques,* Vol. 45, No. 8, 1193–1203, Aug. 1997.